

COVER PAGE

Document downloaded by @DAEL

Sun Nov 29 12:16:34 2026
For personal use

When automatic English translation is provided, only the original document is authentic.
The EAA cannot be held responsible of any translation error

Bibliographical reference

On the Optimization of an Acoustic Resonator Shape with Respect to Acoustic Pressure Amplitude, Milan Cervenka and Michal Bednarik, Acta Acustica **vol. 99** (Number 2), 2013, pp. 183-191

DOI
https://doi.org/10.3813/AAA.918601

Acta Acustica united with Acustica
Vol. 99 (2013) 183 – 191

DOI 10.3813/AAA.918601

On the Optimization of an Acoustic Resonator Shape with Respect to Acoustic Pressure Amplitude

Milan Cervenka, Michal Bednarik
Czech Technical University in Prague, Faculty of Electrical Engineering, Technicka 2, 166 27 Prague 6, Czech Republic. [milan.cervenka, bednarik]@fel.cvut.cz

Summary
This paper deals with the optimization of an acoustic resonator shape in order to maximize acoustic pressure amplitude. The resonator shape is described using the cubic splines which interconnect a set of control points whose positions are determined using an evolutionary algorithm. As an objective function, numerical solution of modified Webster's equation is used. Numerical results show that the optimized resonators are rather simple-shaped, they differ for a piston- or shaker-driving and the fundamental resonance frequencies are lower than in the case of a constant-cross-section resonator. A nonlinear theory is used for assessment of finite-amplitude fields in the optimized resonators.

PACS no. 43.20.Ks, 43.25.Gf

1. Introduction

Many studies so far published have shown that it is possible to generate standing acoustic waves of such high amplitudes which enable their utilization in practical applications.

Gaitan and Atchley [1] showed that introduction of the cross-section variability in a piston-driven resonator can significantly reduce energy transfer from the fundamental to the higher modes, prevent shock-formation and increase amplitude of the standing wave.

Lawrenson *et al.* [2] presented in their experimental paper concept of Resonant Macrosonic Synthesis (RMS) whereby they obtained acoustic pressure amplitude more than an order larger than it had been possible previously. The concept is based on so-called dissonant resonators, whose varying-cross-section cavities don't have the higher eigenfrequencies coincident with the harmonics of the nonlinearly distorted waveform which results in the suppression of a shock-wave formation. The authors demonstrated a strong dependence of obtained maximum amplitude on the resonator shape (cylindrical, conical, horn-cone hybrid and bulb).

Ilinskii *et al.* [3] presented in their theoretical paper a quasi-one-dimensional model equation expressed in terms of the velocity potential for description of high-amplitude standing waves in axi-symmetric but otherwise arbitrarily shaped acoustic resonators. The model comprises nonlinearity, viscous bulk attenuation and entire-resonator driving by an external force (shaker-driving). A numerical algorithm was proposed for integration of the model equation in the frequency domain, the numerical simulations were conducted in the case of a cylindrical, conical and bulb-shaped resonator. The numerical results were in good agreement with the experimental ones. The model was subsequently fulfilled [4] to account for energy losses in the boundary-layer and the losses due to acoustically generated turbulence.

Hamilton *et al.* [5] investigated theoretically dependence of the resonance frequencies of the varying-cross-sectioned resonators and their nonlinear shifts.

Chun and Kim [6] investigated numerically the influence of an entirely-driven resonant cavity shape on the compression ratio (ratio of the maximum and minimum pressure attained at one point in the resonator cavity during one period) using a quasi-one-dimensional model equation based on the conservation laws integrated in the time-domain using a high-order finite-difference scheme. From the several simple shapes (cylindrical, conical, 1/2-cosine and 3/4-cosine) studied, the 1/2-cosine offered the best performance.

Erickson and Zinn [7] developed a Galerkin-method-based algorithm for time-domain integration of the model equation proposed in Ilinskii's *et. al.* paper [3]. They also showed that the exponentially shaped resonator's compression ratio strongly and non-trivially depends on its geometrical parameters.

Luo *et al.* [8] studied theoretically effect of the resonator shape and dimension on its compression ratio in the case of axi-symmetric and low-aspect-ratio exponential geometry, observing its decrease with decreasing resonator length and smaller-radius-to-length ratio.

Received 1 August 2012,
accepted 17 December 2012.

© S. Hirzel Verlag · EAA

Li *et al.* [9] optimized by means of numerical simulations the parameters of simple-shaped resonator cavities in order to maximize the compression ratio. They achieved the value of 48 in the case of an optimized horn-cone shape.

Luo *et al.* [10] conducted numerical experiments in order to compare piston- or entire-driving of exponentially shaped cavity finding similar results.

In all the above-mentioned papers, the same approach was utilized, i.e., the resonator shapes were described using a smooth elementary function with fixed or adjustable (Erickson and Zinn [7], Li *et al.* [9]) parameters, e.g., all the resonator cavities were non-symmetrical, wide at one end and narrow at the other one, where the maximum pressure (or compression ratio) were obtained.

In this paper, a more general approach is used as a starting point. The axi-symmetric resonator shapes are not restricted to a-few-parameter elementary functions, they are rather parametrized using a set of control points which are interconnected using the cubic splines.

The appropriate shapes are determined in order that acoustic pressure at one resonator's end were maximized either in the case of a piston- or shaker-driving. Even if the optimization is performed using a linear theory, the results are verified using a nonlinear model.

Section 2 deals with description of the linearized model equations describing the acoustic field in an axi-symmetric resonator and their solutions. The optimization algorithm is described in section 3. The numerical results are then presented in section 4.

2. Description of Acoustic Field in a Resonator Using Linear Theory

2.1. Model Equation

For description of the acoustic field in a variable-cross-section resonator driven by an external (inertial) force, we can issue from the quasi-one-dimensional model equation derived in [3], which has the form

$$\begin{aligned}\frac{c_0^2}{r^2}\frac{\partial}{\partial x}\left(r^2\frac{\partial\varphi}{\partial x}\right)-\frac{\partial^2\varphi}{\partial t^2}+\frac{\delta}{r^2}\frac{\partial^2}{\partial x\partial t}\left(r^2\frac{\partial\varphi}{\partial x}\right)=\\ x\frac{\mathrm{d}a_\mathrm{s}}{\mathrm{d}t}+a_\mathrm{s}(t)\frac{\partial\varphi}{\partial x}+\frac{\gamma-1}{r^2}a_\mathrm{s}(t)x\frac{\partial}{\partial x}\left(r^2\frac{\partial\varphi}{\partial x}\right)\\ +2\frac{\partial\varphi}{\partial x}\frac{\partial^2\varphi}{\partial x\partial t}+\frac{\gamma-1}{r^2}\frac{\partial\varphi}{\partial t}\frac{\partial}{\partial x}\left(r^2\frac{\partial\varphi}{\partial x}\right)\\ +\frac{1}{3}\frac{\partial}{\partial x}\left(\frac{\partial\varphi}{\partial x}\right)^3+\frac{\gamma-1}{2r^2}\left(\frac{\partial\varphi}{\partial x}\right)^2\frac{\partial}{\partial x}\left(r^2\frac{\partial\varphi}{\partial x}\right),\end{aligned}\tag{1}$$

where φ is the velocity potential, x is the spatial coordinate along the resonator cavity, t is time, $r = r(x)$ is the varying resonator radius, c_0 is small-signal speed of sound, $a_\mathrm{s} = a_\mathrm{s}(t)$ is the driving acceleration (the acceleration with which the entire resonator cavity attached to a shaker oscillates), $\delta = (\zeta + 4\eta/3)/\rho_0$ is an attenuation coefficient, where ζ and η are bulk and shear viscosities, respectively, ρ_0 is ambient fluid density and γ is the Poisson's constant.

After linearization, equation (1) reduces into the form

$$\begin{aligned}\frac{c_0^2}{r^2}\frac{\partial}{\partial x}\left(r^2\frac{\partial\varphi}{\partial x}\right)-\frac{\partial^2\varphi}{\partial t^2}=\\ -\frac{\delta}{r^2}\frac{\partial^2}{\partial t\partial x}\left(r^2\frac{\partial\varphi}{\partial x}\right)+\frac{\mathrm{d}a_\mathrm{s}}{\mathrm{d}t}x.\end{aligned}\tag{2}$$

Left side of equation (2) represents the Webster's equation. In the first approximation, an acoustic pressure p' can be calculated from the velocity potential using formula

$$p' = -\rho_0\frac{\partial\varphi}{\partial t}-\rho_0 a_\mathrm{s}x.\tag{3}$$

For the sake of the subsequent analysis, it is convenient to introduce dimensionless variables, e.g. in form

$$\begin{aligned}&X=\frac{x}{l},\quad T=\omega t,\quad R=\frac{r}{l},\\ &A=\frac{a}{l\omega_0^2},\quad \Phi=\frac{\varphi}{l^2\omega_0},\quad P=\frac{p'}{\pi^2\rho_0c_0^2},\end{aligned}$$

where l is the resonator length, ω is the driving frequency and $\omega_0 = \pi c_0/l$ is the first eigenfrequency for a constant-cross-section resonator. Using these new variables, equations (2) and (3) have the form

$$\begin{aligned}\frac{1}{\pi^2R^2}\frac{\partial}{\partial X}\left(R^2\frac{\partial\Phi}{\partial X}\right)-\Omega^2\frac{\partial^2\Phi}{\partial T^2}=\\ -\frac{G\Omega}{\pi^3R^2}\frac{\partial^2}{\partial T\partial X}\left(R^2\frac{\partial\Phi}{\partial X}\right)+D_\mathrm{s},\end{aligned}\tag{4}$$

where

$$D_\mathrm{s}=\Omega\frac{\mathrm{d}A_\mathrm{s}}{\mathrm{d}T}X,$$

and

$$P=-\Omega\frac{\partial\Phi}{\partial T}-A_\mathrm{s}X,\tag{5}$$

where $\Omega = \omega/\omega_0$ and $G = \pi\omega_0\delta/c_0^2$.

As it is assumed that the resonator cavity has rigid walls and end caps, the boundary conditions for the velocity potential have form

$$V(0,T)=\left.\frac{\partial\Phi}{\partial X}\right|_{X=0}=V(1,T)=\left.\frac{\partial\Phi}{\partial X}\right|_{X=1}=0.\tag{6}$$

If the resonator cavity is driven using a vibrating piston positioned at $X = 1$ (instead of entire-driving) having dimensionless velocity $U_\mathrm{p} = U_\mathrm{p}(T)$, it holds true that in equation (4) $D_\mathrm{s} = 0$ and the inhomogeneous boundary conditions have the form[1]

$$\begin{aligned}V(0,T)&=\left.\frac{\partial\Phi}{\partial X}\right|_{X=0}=0,\\ V(1,T)&=\left.\frac{\partial\Phi}{\partial X}\right|_{X=1}=U_\mathrm{p}.\end{aligned}\tag{7}$$

[1] Within the scope of the linear approximation, it is assumed that the velocity $U_\mathrm{p}(T)$ has such a small amplitude that the position of the piston can be assumed to be constant [$X_\mathrm{p}(T) = 1$].

It is further advantageous to homogenize the boundary conditions (7) introducing new variable $\Psi(X,T)$ obeying relation

$$\Phi = \Psi + \frac{X^2}{2}U_\mathrm{p} \quad \Rightarrow \quad V = \frac{\partial\Phi}{\partial X} = \frac{\partial\Psi}{\partial X} + XU_\mathrm{p} \tag{8}$$

Substituting the relations (8) into equation (4) results in

$$\frac{1}{\pi^2R^2}\frac{\partial}{\partial X}\left(R^2\frac{\partial\Psi}{\partial X}\right) - \Omega^2\frac{\partial^2\Psi}{\partial T^2} = -\frac{G\Omega}{\pi^3R^2}\frac{\partial^2}{\partial T\partial X}\left(R^2\frac{\partial\Psi}{\partial X}\right) + D_\mathrm{p}, \tag{9}$$

where

$$\begin{aligned} D_\mathrm{p} &= -\frac{1}{\pi^2R^2}\frac{\mathrm{d}(XR^2)}{\mathrm{d}X}U_\mathrm{p} + \Omega^2\frac{X^2}{2}\frac{\mathrm{d}^2U_\mathrm{p}}{\mathrm{d}T^2} \\ &\quad - \frac{G\Omega}{\pi^3R^2}\frac{\mathrm{d}(XR^2)}{\mathrm{d}X}\frac{\mathrm{d}U_\mathrm{p}}{\mathrm{d}T} \\ &\approx -\left(1 + \frac{2X}{R}\frac{\mathrm{d}R}{\mathrm{d}X}\right)\frac{U_\mathrm{p}}{\pi^2} + \Omega^2\frac{X^2}{2}\frac{\mathrm{d}^2U_\mathrm{p}}{\mathrm{d}T^2}, \end{aligned} \tag{10}$$

because $G \ll 1$. The boundary conditions for equation (9) then have the form

$$\left.\frac{\partial\Psi}{\partial X}\right|_{X=0} = \left.\frac{\partial\Psi}{\partial X}\right|_{X=1} = 0. \tag{11}$$

If the driving acceleration is harmonic, having the form $A_\mathrm{s}(T) = A_{\mathrm{s}0}\cos(T) = \Re\left[A_{\mathrm{s}0}\exp(\mathrm{i}T)\right]$ and we are only looking for the stationary solutions $\Phi(X,T) = \Re\left[\tilde{\Phi}(X)\exp(\mathrm{i}T)\right]$, then equation (4) can be rewritten into the form

$$\frac{1}{\pi^2R^2}\frac{\mathrm{d}}{\mathrm{d}X}\left(R^2\frac{\mathrm{d}\tilde{\Phi}}{\mathrm{d}X}\right) + \Omega^2\tilde{\Phi} = -\frac{\mathrm{i}G\Omega}{\pi^3R^2}\frac{\mathrm{d}}{\mathrm{d}X}\left(R^2\frac{\mathrm{d}\tilde{\Phi}}{\mathrm{d}X}\right) + \mathrm{i}\Omega A_{\mathrm{s}0}X. \tag{12}$$

Similarly, equation (9) can be recast into the form

$$\begin{aligned} &\frac{1}{\pi^2R^2}\frac{\mathrm{d}}{\mathrm{d}X}\left(R^2\frac{\mathrm{d}\tilde{\Psi}}{\mathrm{d}X}\right) + \Omega^2\tilde{\Psi} = \\ &-\frac{\mathrm{i}G\Omega}{\pi^3R^2}\frac{\mathrm{d}}{\mathrm{d}X}\left(R^2\frac{\mathrm{d}\tilde{\Psi}}{\mathrm{d}X}\right) \\ &-\left(1 + \frac{2X}{R}\frac{\mathrm{d}R}{\mathrm{d}X} + \pi^2\Omega^2\frac{X^2}{2}\right)\frac{U_{\mathrm{p}0}}{\pi^2}. \end{aligned} \tag{13}$$

2.2. Solution of the Model Equations

Equations (12) and (13) can be solved using the method of eigenfunction expansions [11]. Nontrivial solutions $\{F_k, k = 1, 2, \dots\}$ of equation (Sturm-Liouville problem)

$$\frac{1}{\pi^2R^2}\frac{\mathrm{d}}{\mathrm{d}X}\left(R^2\frac{\mathrm{d}F}{\mathrm{d}X}\right) + \Omega^2F = 0 \tag{14}$$

with homogeneous boundary conditions

$$\left.\frac{\mathrm{d}F}{\mathrm{d}X}\right|_{X=0} = \left.\frac{\mathrm{d}F}{\mathrm{d}X}\right|_{X=1} = 0$$

exist for certain values (eigenfrequencies) $\{\Omega_k\}$. These eigenfunctions (eigenmodes) are orthogonal for individual eigenfrequencies Ω_k, which in this case means that

$$\left\langle F_k|F_j\right\rangle = \int_0^1 R^2(X)F_k(X)F_j(X)\,\mathrm{d}X = 0 \tag{15}$$

for $k \neq j$ and because the functions $\{F_k\}$ form a complete set, the solution of equation (12) can be written as

$$\tilde{\Phi}(X) = \sum_{k=1}^{\infty}\tilde{\alpha}_kF_k(X), \tag{16}$$

where $\tilde{\alpha}_k$ are complex coefficients. Substituting the above relation into equation (12) yields

$$\sum_{k=1}^{\infty}\left(\pi\Omega^2 - \pi\Omega_k^2 - \mathrm{i}G\Omega\Omega_k^2\right)\tilde{\alpha}_kF_k = \mathrm{i}\pi\Omega A_{\mathrm{s}0}X.$$

Multiplication of both the sides of the above equation by function R^2F_j, integration in limits $\langle 0,1\rangle$ with respect to X and utilization of the orthogonality relation yields

$$\tilde{\alpha}_j = \frac{\mathrm{i}\pi\Omega A_{\mathrm{s}0}}{\pi\Omega^2 - \pi\Omega_j^2 - \mathrm{i}G\Omega\Omega_j^2}\frac{\langle X|F_j\rangle}{\langle F_j|F_j\rangle}. \tag{17}$$

Substitution of equation (17) into equation (16) then results in the solution of equation (12) in the form

$$\tilde{\Phi}(X) = \mathrm{i}\pi\Omega A_{\mathrm{s}0}\sum_{j=1}^{\infty}\frac{\langle X|F_j\rangle F_j(X)}{(\pi\Omega^2 - \pi\Omega_j^2 - \mathrm{i}G\Omega\Omega_j^2)\langle F_j|F_j\rangle}. \tag{18}$$

Because $G \ll 1$, for $\Omega = \Omega_j$ (at resonance) the result can be simplified as

$$\tilde{\Phi}(X, \Omega = \Omega_j) \approx -\frac{\pi A_{\mathrm{s}0}}{G\Omega_j^2}\frac{\langle X|F_j\rangle}{\langle F_j|F_j\rangle}F_j(X). \tag{19}$$

Application of the same procedure to equation (13) yields in

$$\begin{aligned} \tilde{\Phi}(X) = &\frac{\mathrm{i}A_{\mathrm{p}0}}{\pi\Omega}\sum_{j=1}^{\infty}\frac{\langle 1 + 2X(\mathrm{d}R/\mathrm{d}X)/R + \pi^2\Omega^2X^2/2|F_j\rangle F_j(X)}{(\pi\Omega^2 - \pi\Omega_j^2 - \mathrm{i}G\Omega\Omega_j^2)\langle F_j|F_j\rangle} \\ &- \frac{\mathrm{i}A_{\mathrm{p}0}X^2}{2\Omega}, \end{aligned} \tag{20}$$

where $A_{\mathrm{p}0} = \mathrm{i}\Omega U_{\mathrm{p}0}$ is a dimensionless amplitude of acceleration of the driving piston. At the resonance, equation (20) reduces to

$$\begin{aligned} \tilde{\Phi}(X, \Omega = \Omega_j) \approx &-\frac{A_{\mathrm{p}0}}{\pi G\Omega_j^4}\frac{\langle 1 + 2X(\mathrm{d}R/\mathrm{d}X)/R + \pi^2\Omega_j^2X^2/2|F_j\rangle}{\langle F_j|F_j\rangle}F_j(X) \\ &- \frac{\mathrm{i}A_{\mathrm{p}0}X^2}{2\Omega_j}. \end{aligned} \tag{21}$$

2.3. Finding the Eigenmodes and Eigenfrequencies

Nontrivial solutions of equation (14) are known in an analytical form for some functions $R(X)$ (constant, linear, exponential, ...), in the other cases, they can be looked for numerically [12]. The equation (14) can be rewritten into the form

$$\frac{\mathrm{d}F}{\mathrm{d}X} = \frac{W}{R^2}, \qquad \frac{\mathrm{d}W}{\mathrm{d}X} = -\pi^2\Omega^2 R^2 F \tag{22}$$

and integrated numerically [12] with initial conditions $\{F(0) = 1, W(0) = 0\}$. An eigenfrequency Ω_k is calculated numerically as a solution of the following equation

$$W(X = 1; \Omega_k) = 0, \qquad \Omega_k \in \langle \Omega_{\min}, \Omega_{\max} \rangle. \tag{23}$$

Once the eigenfrequency Ω_k is known, the corresponding eigenfunction F_k is also known, because it is the solution of equation (22) with the corresponding initial conditions and $\Omega = \Omega_k$.

3. Optimization of the Resonator Shape

3.1. Description of the Resonator Shape and Its Eligibility

So as not to restrict the resonator's shape to a specific predefined elementary function with only a few adjustable parameters, it is defined using N control points distributed regularly at positions

$$X_i = \frac{i}{N-1}, \qquad i = 0, 1, \ldots, N-1,$$

whose corresponding values $R(X_i) = R_i$ are found in predefined interval $R_i \in \langle R_{\min}, R_{\max} \rangle$.

The function $R(X)$ is obtained using the cubic-spline-interpolation of the control points (the function and its first and second derivatives are continuous) with zero derivatives at the ends of the interval. The values R_i are chosen in order that $R_{\min} \le R(X) \le R_{\max}$ for any $X \in \langle 0, 1 \rangle$.

With the resonator shape defined, an eigenfrequency Ω_k is looked for numerically in an interval $\langle \Omega_{\min}, \Omega_{\max} \rangle$ using equation (23). If there is not any solution found, the control-points set is rejected and a new set of values R_i is generated and the procedure repeats.

Once an eigenfrequency Ω_k is found, corresponding eigenmode $F_k(X)$ is also known as it is a solution of equations (22) for $\Omega = \Omega_k$. With use of this information, a suitable objective function can be evaluated for assessment of the resonator shape eligibility (quality).

As an objective function, the acoustic pressure amplitude at $X = 0$ is chosen. In the sake of a shaker-driven resonator we can, using equations (19) and (5), write

$$P_{\mathrm{s}0} = K_{\mathrm{s}} \frac{|A_{\mathrm{s}0}|}{G}, \text{ where } K_{\mathrm{s}} = \frac{\pi}{\Omega_k} \left| \frac{\langle X | F_k \rangle}{\langle F_k | F_k \rangle} F_k(0) \right|, \tag{24}$$

thus the resonator shape is searched for in order that the quantity K_{s} (which will be called in the following text as the *eligibility factor*) were maximized. In the case of a piston-driven resonator, we can similarly [using equations (21) and (5)] write

$$P_{\mathrm{p}0} = K_{\mathrm{p}} \frac{|A_{\mathrm{p}0}|}{G}, \tag{25}$$

$$K_{\mathrm{p}} = \frac{1}{\pi\Omega_k^3} \cdot \left| \frac{\langle 1 + 2X(\mathrm{d}R/\mathrm{d}X)/R + \pi^2\Omega_k^2 X^2/2 | F_k \rangle}{\langle F_k | F_k \rangle} F_k(0) \right|.$$

Again, the resonator shape is searched for in order that the eligibility factor K_{p} were maximized.

The above-described procedure is schematically depicted in Figure 1.

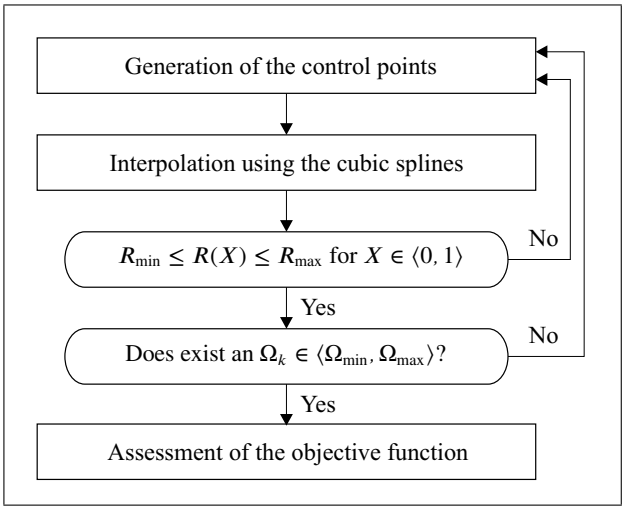

Figure 1. Flowchart of the algorithm for assessment of the resonator shape eligibility.

3.2. The Optimization Method

As the parameter search space for the objective function is many- (N-) dimensional ($\mathbb{R}^N$) and moreover, it is not continuous (some control-points sets lead to $R(X)$ that does not lie in pre-defined interval $\langle R_{\min}, R_{\max} \rangle$, possibly there is no eigenfrequency $\Omega_k \in \langle \Omega_{\min}, \Omega_{\max} \rangle$), a heuristic optimization method seems to have reasonable use for this type of problem. In this concrete case, a variant of Evolution Strategies [13] $(\mu + \lambda)$-ES was utilized.

The algorithm works as follows. Firstly, a population of M parents (randomly-generated sets of control points) is generated. For each member of the population, its objective function is evaluated according to the procedure described in Figure 1. Then, μ members with the highest values of the objective function are used as parents for the next generation. Each of the μ parents generates μ offspring by mutation (addition of a random number with Gaussian distribution and standard deviation σ (mutation strength) to individual R_i) using the formula

$$R_{i\mathrm{offspring}} = R_{i\mathrm{parent}} + \sigma\mathcal{N}_i(0, 1), \qquad i = 0, 1, \ldots, N-1.$$

These $\lambda = \mu \times \mu$ offspring together with their μ parents are supplemented with $M - \mu(\mu+1)$ randomly generated specimen, all these are evaluated and the cycle repeats. During

the evolution, the mutation strength σ is slowly decreased in order to maintain the algorithm effective.

4. Numerical Results

4.1. Optimization of the Resonator Shape

Within the numerical experiments, the resonant cavities were parametrized using $N = 10$ control points. As it seems to be reasonable to suppose that for the fixed number of control points, the maximum resonator eligibility factor depends on the ratio of minimum and maximum radius, the resonant cavities were optimized for $R_{\min}/R_{\max} = 2/5$ and $1/5$, both, for shaker and piston driving.

In all the cases, parameters of the evolutionary algorithm were set as follows: $M = 500$, $\mu = 20$, evolution ran for 500 generations with the mutation strength decreasing from $\sigma_1 = 0.01$ to $\sigma_2 = 0.0001$. In all the cases, the algorithm was run repeatedly many rimes with reached dispersion of the maximized objective function in a level of fractions of one percent.

The numerical results are summarized in Table I and in Figures 2–7. For comparison, results for a constant-cross-section resonator and a conical resonator with $R_{\min}/R_{\max} = 1/9$ (similar to the one presented by Ilinskii *et al.* [3]) are included.

In the case of the constant-cross-section resonator, the eligibility factor for the shaker-driven resonator attains value of $K_s = 1.27$, the one for the piston driving $K_p = K_s/2$, which means, that with the same acceleration amplitude, the piston-driving provides half an acoustic pressure amplitude than in the case of the shaker-driving. Major disadvantage of this simple shape is the fact, that the higher eigenfrequencies are the integer multiples of the fundamental eigenfrequency which results in substantial nonlinear distortion in the high-amplitude fields and evolution of the shock-wave.

In the case of the conical resonator, see Table I, the factors K_s and K_p attain higher values than in the previous case and again, the shaker-driving is more effective. What is also important is the fact that the higher eigenfrequencies are not the integer multiples of the eigenfrequency fundamental, so that the nonlinearly generated higher harmonics are not coincident with the eigenfrequencies and thus they are suppressed. The shape of the resonator cavity and the first eigenmode are depicted in Figure 2.

The shapes of the acoustic resonators with $R_{\min}/R_{\max} = 2/5$ optimized for shaker- and piston-driving together with the corresponding eigenmodes are shown in Figure 3, the eligibility factors and eigenfrequencies are summarized in the second row of Table I. The optimum shapes were searched for in the frequency interval $\Omega \in \langle 0.2, 2.0 \rangle$ in all the cases.

In both the cases, the optimum resonator shapes are rather simple and similar, they have the maximum allowed radius at both the ends, the resonator optimized for a piston-driving is symmetric. Due to the frequency-dependence of the viscous attenuation, the optimum shapes are

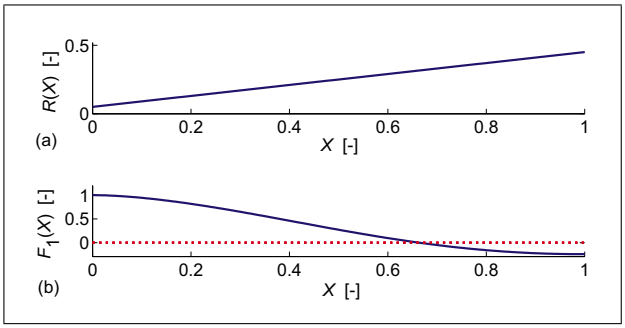

Figure 2. Conical cavity with $R_{\min}/R_{\max} = 1/9$, $\Omega_1 = 1.282$. (a) Cavity shape, (b) Eigenmode shape.

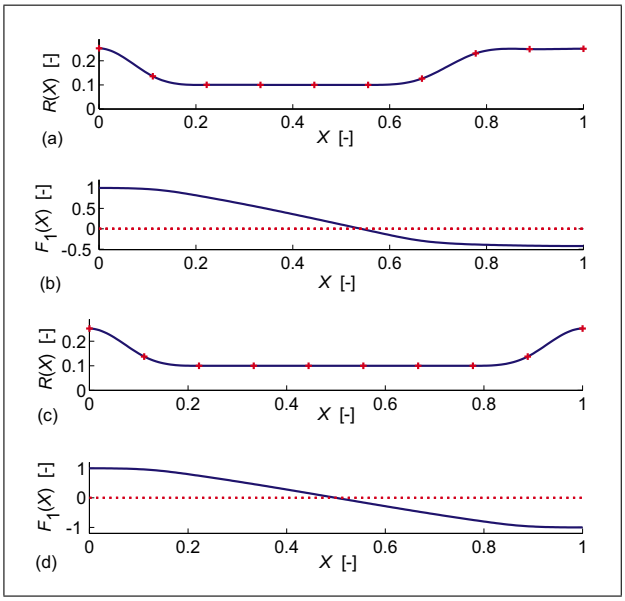

Figure 3. Optimized resonator shapes and corresponding eigenmodes for $R_{\min}/R_{\max} = 2/5$. (a,b): optimization for a shaker driving, $\Omega_1 = 0.606$; (c,d): optimization for a piston driving, $\Omega_1 = 0.642$. (a) Cavity shape (shaker-optimized), (b) Eigenmode shape (shaker-optimized), (c) Cavity shape (piston-optimized), (d) Eigenmode shape (piston-optimized).

connected with very low fundamental eigenfrequencies ($\Omega_1 = 0.606$ in the shaker- and $\Omega_1 = 0.642$ in the piston-driving case). In both the cases, the higher eigenfrequencies are not integer multiples of the fundamental eigenfrequencies, which is important in the case of high-amplitude fields. The eligibility factors in Table I show that piston-driving is more effective even if the resonator is optimized for the shaker-driving, the maximum eligibility factor $K_p = 6.08$ in the case of piston-driven piston-optimized resonator, which is 9.6× more than in the case of a piston-driven cylindrical resonator.

Similarly, shapes of the acoustic resonators with $R_{\min}/R_{\max} = 1/5$ optimized for a shaker- or piston-driving together with the corresponding fundamental eigenmodes are shown in Figure 4, the eligibility factors and eigenfrequencies are summarized in the third row of Table I. Comparison of Figures 3 and 4 reveals that the optimum-resonator shapes are very similar as in the pre-

Table I. Parameters of individual resonant cavities.

Cylindrical, $R(X) = const.$ $K_s = 1.27,\ K_p = K_s/2,\ \Omega_i = 1, 2, 3, 4, 5, \ldots$	Conical, $R_{min}/R_{max} = 1/9$ $K_s = 1.77,\ K_p = 1.14,\ \Omega_i = 1.28, 2.23, 3.19, 4.15, 5.13, \ldots$
Opt. for shaker, $R_{min}/R_{max} = 2/5$ $K_s = 2.98,\ K_p = 4.09,\ \Omega_i = 0.61, 1.90, 3.14, 3.90, 5.05, \ldots$	Opt. for piston, $R_{min}/R_{max} = 2/5$ $K_s = 2.14,\ K_p = 6.08,\ \Omega_i = 0.64, 1.61, 2.75, 3.93, 5.07, \ldots$
Opt. for shaker, $R_{min}/R_{max} = 1/5$ $K_s = 5.46,\ K_p = 20.43,\ \Omega_i = 0.36, 1.95, 3.43, 3.96, 5.41, \ldots$	Opt. for piston, $R_{min}/R_{max} = 1/5$ $K_s = 3.69,\ K_p = 38.38,\ \Omega_i = 0.38, 1.48, 2.78, 4.08, 5.33, \ldots$
Opt. for shaker, $R_{min}/R_{max} = 2/5, \Omega_1 = 1$ $K_s = 2.27,\ K_p = 1.15,\ \Omega_i = 1.00, 1.82, 3.03, 3.90, 4.99, \ldots$	Opt. for piston, $R_{min}/R_{max} = 2/5, \Omega_1 = 1$ $K_s = 1.68,\ K_p = 2.85,\ \Omega_i = 1.00, 1.50, 3.10, 3.58, 5.12, \ldots$
Opt. for shaker, $R_{min}/R_{max} = 1/5, \Omega_1 = 1$ $K_s = 3.03,\ K_p = 2.05,\ \Omega_i = 1.00, 1.34, 3.37, 4.20, 5.13, \ldots$	Opt. for piston, $R_{min}/R_{max} = 1/5, \Omega_1 = 1$ $K_s = 2.18,\ K_p = 6.65,\ \Omega_i = 1.00, 1.19, 3.01, 4.08, 5.22, \ldots$

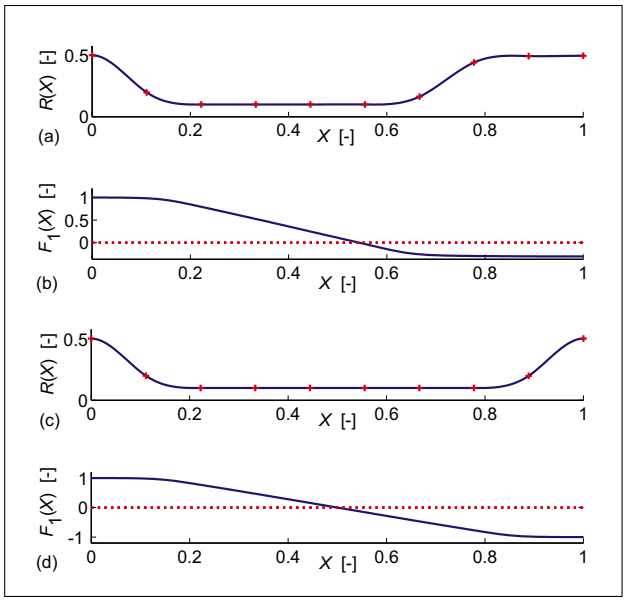

Figure 4. Optimized resonator shapes and corresponding eigenmodes for $R_{min}/R_{max} = 1/5$. (a,b): optimization for a shaker driving, $\Omega_1 = 0.361$; (c,d): optimization for a piston driving, $\Omega_1 = 0.382$. (a) Cavity shape (shaker-optimized), (b) Eigenmode shape (shaker-optimized), (c) Cavity shape (piston-optimized), (d) Eigenmode shape (piston-optimized).

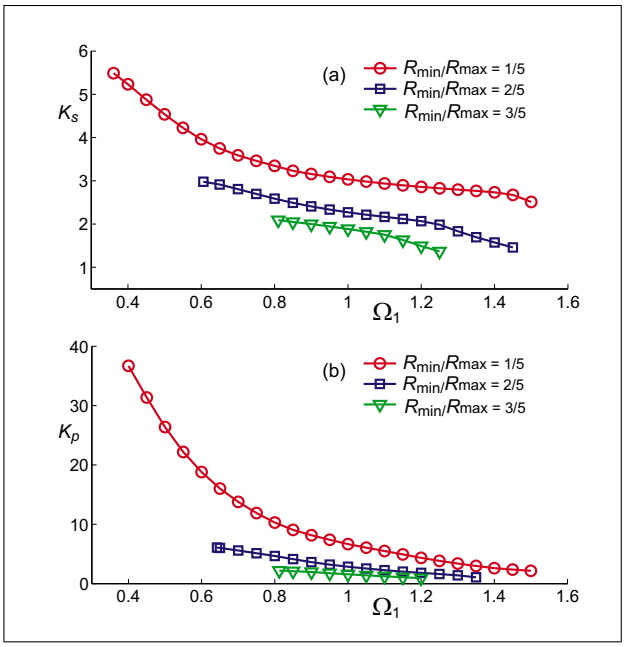

Figure 5. Eligibility factors for different ratios R_{min}/R_{max} optimized in individual frequency intervals delimited by a minimum frequency Ω_1. (a) Shaker-optimized, shaker-driving, (b) Piston-optimized, piston-driving.

vious case. In this case, the higher ratio of the maximum and minimum radii allows further decrease of the fundamental eigenfrequencies ($\Omega_1 = 0.361$ in the shaker- and $\Omega_1 = 0.382$ in the piston-driving case). Again, the higher eigenfrequencies are not integer multiples of the fundamental ones and the piston driving is more efficient than the shaker driving, the eligibility factor for the piston-optimized piston-driven resonator attains value of $K_p = 38.38$. Comparison of the eligibility factors in Table I clearly reveals, that increase of the ratio R_{max}/R_{min} results in much bigger increase of the eligibility factor for the piston-driven resonator than for the shaker-driven one.

In some cases, the low eigenfrequencies of the optimum-shaped cavities need not be preferable. If the resonator shape is optimized in the frequency range $\Omega \in \langle \Omega_{min}, \Omega_{max} \rangle$, where $\Omega_{min} > \Omega_{opt}$, the algorithm finds quasi-optimum shape with eigenfrequency $\Omega = \Omega_{min}$, however, the appropriate eligibility factor is smaller than in the case of the optimum-shaped resonator. The dependence of the eligibility factor on the lowest allowed frequency for individual R_{min}/R_{max} ratios are depicted in Figure 5. It can be seen in all the cases that the lower $\Omega_{min} > \Omega_{opt}$ is allowed, the higher eligibility factor is attained. Higher ratio R_{max}/R_{min} always causes higher eligibility factor for the given frequency. It can be observed in Figure 5 that the frequency-dependence of the eligibility factor value increases with R_{max}/R_{min} ratio and the increase is stronger in the case of a piston-driven resonator.

In Figures 6 and 7 there are the quasi-optimum resonator shapes and the corresponding fundamental eigenmodes depicted for $\Omega_{min} = \Omega_1 = 1$. The corresponding eligibility factors and the eigenfrequencies can be found

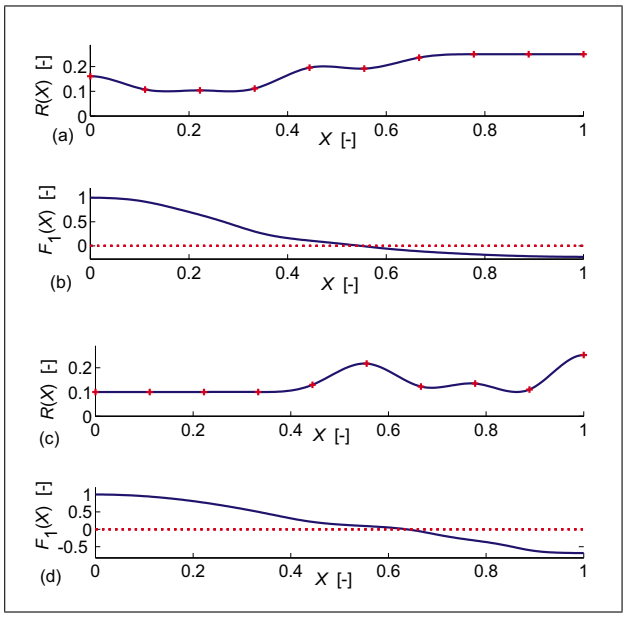

Figure 6. Quasi-optimum resonator shapes and corresponding eigenmodes for $R_{\min}/R_{\max} = 2/5$. (a,b): optimization for a shaker driving, (c,d): optimization for a piston driving, in both the cases $\Omega_1 = 1$. (a) Cavity shape (shaker-optimized), (b) Eigenmode shape (shaker-optimized), (c) Cavity shape (piston-optimized), (d) Eigenmode shape (piston-optimized).

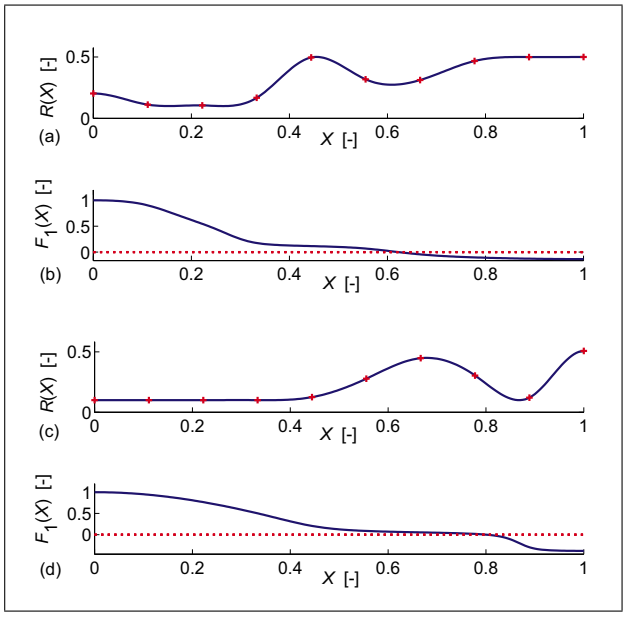

Figure 7. Quasi-optimum resonator shapes and corresponding eigenmodes for $R_{\min}/R_{\max} = 1/5$. (a,b): optimization for a shaker driving, (c,d): optimization for a piston driving, in both the cases $\Omega_1 = 1$. (a) Cavity shape (shaker-optimized), (b) Eigenmode shape (shaker-optimized), (c) Cavity shape (piston-optimized), (d) Eigenmode shape (piston-optimized).

in the last two rows in Table I. It can be observed that in these cases, the resonator shapes are slightly more complicated. Again, the higher eigenfrequencies are not integer multiples of the fundamental ones. Moreover, driving the resonator cavity in different way than it was designed for, results in significant decrease of the eligibility factor.

4.2. Finite-amplitude Acoustic Field in Optimized Resonators

High-amplitude acoustic fields were studied using the nonlinear model equation (1) proposed by Ilinskii *et al.* [3]. As in the original paper, the model equation was integrated numerically in the frequency domain; the two-point boundary value problem was solved using the shooting method, see e.g. [12].

As medium, air at normal atmospheric conditions was assumed ($\rho_0 = 1.2\,\mathrm{kg/m^3}$, $c_0 = 345\,\mathrm{m/s}$, $\gamma = 1.4$). The value of the attenuation coefficient $G = 10^{-2}$ was used [3, 9].

Figure 9 shows the frequency characteristics (amplitude of the fundamental harmonics at $X = 0$ – one-sided spectrum) of the piston-optimized piston-driven acoustic resonator with $R_{\min}/R_{\max} = 2/5$ (see Figure 8 c)) for different piston acceleration amplitudes. The frequency characteristics exhibits softening behavior with hysteresis for higher driving accelerations.

Figure 10 (top) shows distribution of amplitudes of the first three harmonics of acoustic pressure along the same resonator as in the previous case for $A_{\mathrm{p0}} = 5 \times 10^{-4}$ and $\Omega = 0.586$. This frequency is reached using slow downwards frequency-sweep, at this point, maximum amplitude of the acoustic pressure is attained (see Figure 9). The small-amplitude resonance frequency for this resonator (see above) is $\Omega_{\mathrm{lin}} = 0.642$. It can be seen that the acoustic field is strongly nonlinearly distorted and that the 2nd harmonics attains similar amplitudes as the fundamental one. The bottom part of the figure shows distribution of the static (dc) pressure change caused by the nonlinear effects. The static pressure increases by 5 kPa at the ends of the resonator cavity and decreases by 7.5 kPa at its center.

Figure 11 shows for comparison the same data as Figure 10 but for a conical resonator with $R_{\min}/R_{\max} = 1/9$ (see Figure 8 b)) driven at the resonance frequency $\Omega = 1.285$ with the piston acceleration amplitude $A_{\mathrm{p0}} = 5 \times 10^{-4}$. It can be observed that the 1st harmonics attains approximately half an amplitude at $X = 0$ compared with the optimized resonator and the higher harmonics are much less developed. Due to this fact, the dc pressure change is also smaller (it attains $\Delta p_{\mathrm{dc}} = 1.2\,\mathrm{kPa}$, compared with $\Delta p_{\mathrm{dc}} = 12.5\,\mathrm{kPa}$ in the case of the optimized resonator).

5. Discussion

An optimization algorithm was proposed for maximizing the standing-wave acoustic pressure amplitude by shaping of axi-symmetric resonator cavities. The algorithm is based on the Webster's equation supplemented with a term including viscous attenuation and driving. Within this model, there is one important parameter ($R_{\min}/R_{\max}$ ratio) affecting the acoustic field properties.

It has been shown that the optimum resonators are rather simple-shaped, symmetric in the case of the piston-driving

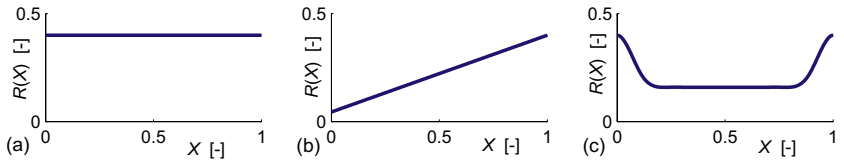

Figure 8. Comparison of shapes of resonators: (a) constant-cross-section resonator, (b) conical resonator, (c) resonator optimized for piston-driving.

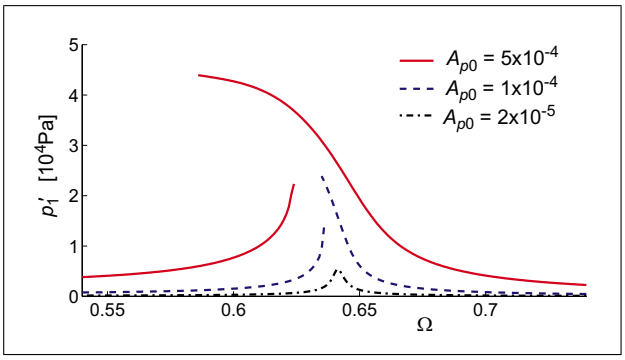

Figure 9. Frequency characteristics of the piston-optimised piston-driven resonator with $R_{\min}/R_{\max} = 2/5$ for different driving acceleration amplitudes A_{p0}.

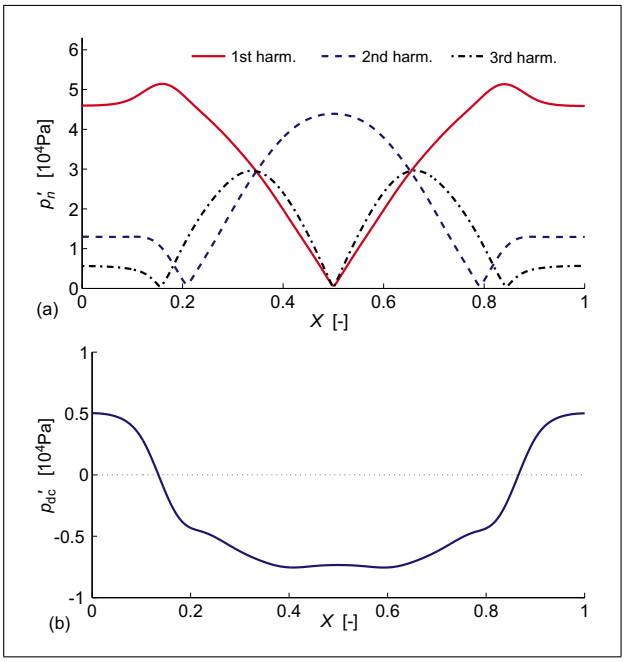

Figure 10. Top: distribution of acoustic pressure amplitude spectrum (one-sided) along the optimized-resonator axis; bottom: distribution of dc-pressure change (piston-optimized, piston-driven, $A_{\mathrm{p0}} = 5 \times 10^{-4}$, $\Omega = 0.586$). (a) Individual harmonics, (b) DC pressure change.

and non-symmetric in the case of the shaker-drivng. In both the cases, the optimum shape shifts the resonant frequency downwards (compared with a cylindrical resonator, where $\Omega_1 = 1$), the resonance frequency is the lower, the lower the ratio $R_{\min}/R_{\max}$ is. This behavior can be advantageous for practical applications, because for the given frequency (in Hertz), the resonant cavity length

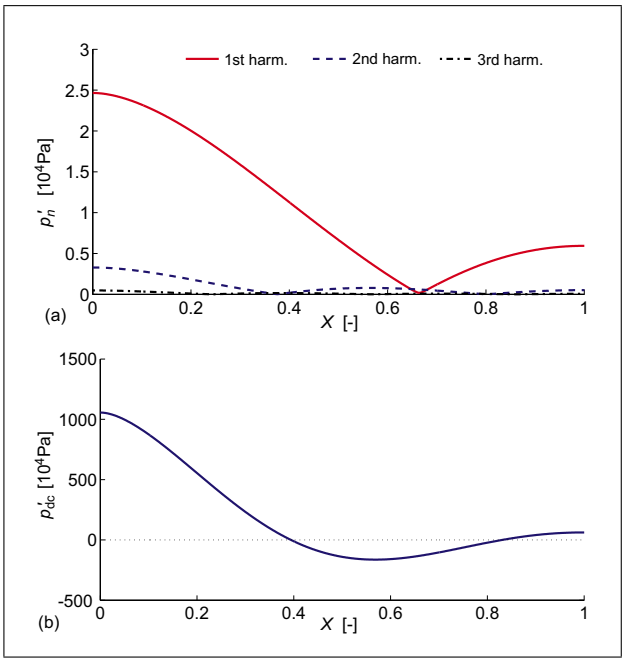

Figure 11. Top: distribution of acoustic pressure amplitude spectrum (one-sided) along the conical-resonator ($R_{\min}/R_{\max} = 1/9$) axis; bottom: distribution of dc-pressure change (piston-driven, $A_{\mathrm{p0}} = 5 \times 10^{-4}$, $\Omega = 1.285$). (a) Individual harmonics, (b) DC pressure change.

is smaller and for the given resonant cavity length, the resonance frequency is lower which can be applicable in pumping applications, where fast valves are used. The numerical results also show that optimum driving is always connected with driving of the lowest (fundamental) mode.

It has been shown that the piston driving gives rise to higher acoustic pressure amplitudes than the shaker driving when the optimized resonant cavities are used with the same driving acceleration amplitudes. Even if the shaker-driven cavity is technically much simpler in the concrete applications (there is no need of tightening of the moving piston), it requires more powerful (and thus more expensive) driving system. Replacement of the moving piston with e.g. a horn-driver thus seems to show a direction to low-cost applications utilizing high-amplitude acoustic fields.

Conducted numerical experiments indicate that the optimized acoustic resonators provide high-amplitude acoustic fields also in the nonlinear regime, even if the higher harmonics components are excited. The nonlinear interactions, on the other hand, generate strong change of the static pressure along the resonator axis which can be utilized in no-valve pumping of fluids.

It is important to emphasize that the used model is rather simplified, e.g., all the dissipation mechanisms are included in an experimentally justified [3, 9] parameter G. However, this approach allows to formulate simple results which have, on the other hand, limited validity. In the future work, the authors intend to propose more realistic optimization model including the dissipation effect of the boundary layer as well as the non-acoustic dissipation mechanisms. The interest will be e specially focused on the optimization of a complex system consisting of a resonant cavity connected to a horn-driver.

Acknowledgments

This work has been supported by GA CR grant project P101/12/1925.

References

[1] D. F. Gaitan, A. A. Atchley: Finite amplitude standing waves in harmonic and anharmonic tubes. J. Acoust. Soc. Am. **93** (1993) 2489–2495.

[2] C. C. Lawrenson, B. Lipkens, T. S. Lucas, D. K. Perkins, T. W. Van Doren: Measurements of macrosonic standing waves in oscillating closed cavities. J. Acoust. Soc. Am. **104** (1998) 623–636.

[3] Y. A. Ilinskii, B. Lipkens, T. S. Lucas, T. W. Van Doren, E. A. Zabolotskaya: Nonlinear standing waves in an acoustical resonator. J. Acoust. Soc. Am. **104** (1998) 2664–2674.

[4] Y. A. Ilinskii, B. Lipkens, E. A. Zabolotskaya: Energy losses in an acoustical resonator. J. Acoust. Soc. Am. **109** (2001) 1859–1870.

[5] M. F. Hamilton, Y. A. Ilinskii, E. A. Zabolotskaya: Linear and nonlinear frequency shifts in acoustical resonators with varying cross sections. J. Acoust. Soc. Am. **110** (2001) 109–119.

[6] Y.-D. Chun, Y.-H. Kim: Numerical analysis for nonlinear resonant oscillations of gas in axisymmetric closed tubes. J. Acoust. Soc. Am. **108** (2000) 2765–2774.

[7] R. R. Erickson, B. T. Zinn: Modeling of finite amplitude acoustic waves in closed cavities using the Galerkin method. J. Acoust. Soc. Am. **113** (2003) 1863–1870.

[8] C. Luo, X. Y. Huang, N. T. Nguyen: Effect of resonator dimensions on nonlinear standing waves. J. Acoust. Soc. Am. **117** (2005) 96–103.

[9] X. Li, J. Finkbeiner, G. Raman, C. Danielsb, B. M. Steinetz: Optimized shapes of oscillating resonators for generating high-amplitude pressure waves. J. Acoust. Soc. Am. **116** (2004) 2814–2821.

[10] C. Luo, X. Y. Huang, N. T. Nguyen: Generation of shock-free pressure waves in shaped resonators by boundary driving. J. Acoust. Soc. Am. **121** (2007) 2515–2521.

[11] D. Zwillinger: Handbook of differential equations. Academic Press, San Diego, 1997.

[12] W. H. Press, S. A. Teukolsky, W. T. Vetterling, B. P. Flannery: Numerical recipes 3rd edition: The art of scientific computing. Cambridge University Press, Cambridge, 2007.

[13] A. E. Eiben, J. E. Smith: Introduction to evolutionary computing. Springer, Berlin, 2010.